Metamagnetic transitions and magnetoelectric coupling in acentric and nonpolar Pb_2MnO_4

D. Chandrasekhar Kakarla,[1,2] H. C. Wu,[1,3] D. J. Hsieh,[1] P. J. Sun,[1] G. J. Dai,[4] J.-Y. Lin,[4,5] J. L. Her,[6] Yasuhiro H. Matsuda,[7] L. Z. Deng,[3] M. Gooch,[3] C. W. Chu,[3,8] and H. D. Yang[1,2,*]

[1]*Department of Physics, National Sun Yat-sen University, Kaohsiung 804, Taiwan*
[2]*Center of Crystal Research, National Sun Yat-sen University, Kaohsiung 804, Taiwan*
[3]*Texas Center for Superconductivity and Department of Physics, University of Houston, Houston, Texas 77204, USA*
[4]*Institute of Physics, National Chiao Tung University, Hsinchu 30010, Taiwan*
[5]*Center for Emergent Functional Matter Science, National Chiao Tung University, Hsinchu 30010, Taiwan*
[6]*Division of Natural Science, Center for General Education, Chang Gung University, Tao-Yuan 333, Taiwan*
[7]*Institute for Solid State Physics, University of Tokyo, 5-1-5 Kashiwanoha, Kashiwa, Chiba 277-8581, Japan*
[8]*Lawrence Berkeley National Laboratory, Berkeley, California 94720, USA*

(Received 26 October 2018; revised manuscript received 5 April 2019; published 16 May 2019)

Acentric and nonpolar Pb_2MnO_4 was predicted to exhibit unique multipiezo induced magnetoelectric (ME) phenomena. In this paper, we present the results of magnetization as well as dielectric properties as a function of temperature (T), magnetic field (H), pressure (P), and electric field (E) primarily to address the ME coupling and identify the underlying mechanism behind this phenomenon. Magnetization and specific-heat measurements reveal the antiferromagnetic ordering of Mn^{4+} spins at temperature $T_N = 17$ K. Metamagnetic transitions at three critical magnetic fields (H_{c1}, H_{c2}, and H_{c3}) are observed for $T < T_N$ and $H > 3.5$ T. Further, the influences of pressure and magnetic field on H_{c1} and H_{c2} are investigated. The T_N, H_{c1}, and H_{c2} all decrease with increasing external pressure. The dielectric anomaly observed at T_N is influenced by applying a magnetic field of $H >$ 3.5 T. However, the electric field has minimal influence on the metamagnetic transition. The scaling between dielectric constant and magnetization meaningfully resolves the existence of magnetic-field-induced higher-order ME coupling in Pb_2MnO_4 at $T < T_N$ and $H > 3.5$ T.

DOI: 10.1103/PhysRevB.99.195129

I. INTRODUCTION

Magnetoelectric (ME) materials manifest a magnetic (electric) polarization with the application of an external electric (magnetic) field and have been anticipated to create multifunctional devices in the field of spintronics as well as the data storage industry [1,2]. Their uniqueness comes from the coupling between the magnetic and electronic degrees of freedom, which has also increased fundamental physics research [3]. Therefore, an in-depth understanding of the mechanism(s) behind such an exotic phenomenon has considerable implications, especially from a device perspective.

To date, several materials have proven to possess spin induced multiferroicity, and many diverse mechanisms have been proposed to justify the origin of the observed effects [4–10]. Among them, Dzyaloshinskii-Moriya interaction accounts for the origin of ferroelectricity in spiral magnetic systems [5]. On the other hand, exchange striction adequately explains the ferroelectricity in the quasicollinear spin arrangement [11]. Extensive research efforts have led to the discovery of many novel materials such as skyrmions, oxyhalides, organic-inorganic compounds, two-dimensional layer materials, and simple binary oxides [12–17]. ME coupling by spin-lattice interaction is a widespread mechanism in the field of multiferroics, where the spin-lattice coupling results in a higher-order ME, which was investigated by magnetodielectric (MD) measurements [12,18–25]. It is well known that several antiferromagnetic (AFM) materials such as MnO, MnF_2, and $BaMnF_4$ display significant change of dielectric constant associated with the AFM magnetic ordering [12,20,26,27]. Interestingly, the existence of ME coupling has been established in the simple binary perovskite $\alpha-Mn_2O_3$, where magnetoelastic coupling connects the local lattice distortions with the magnetic sublattice and drives the ME coupling in this system [14].

The phase diagram of the PbO-MnO-O system has received much interest recently due to the lone pair electric dipole of Pb^{2+} ions along with the magnetism of Mn^{4+} ions [28]. Hosting of lone pair ions in the magnetic lattice is a prerequisite to the ME effect. Pb_2MnO_4 is believed to be a promising system because of its crystal structure [29]. Pb_2MnO_4 belongs to the multipiezo crystal class with the space group $P\bar{4}2_1c$, which provides a unique platform to explore the unusual ME phenomenon by external perturbations like magnetic and electric fields and pressures, while the stress induced multiferroic mechanism has yet to be validated with the support of experimental results. The magnetic structure is known to consist of an antiparallel alignment of zigzag chains of the edge-shared Mn octahedra running along the crystallographic c axis [29]. A long-range three-dimensional (3D) AFM ordering is established despite its one-dimensional Mn spin chain [29]. However, to date, no direct evidence of ME coupling has been reported. In this paper we report promising evidence of the higher-order ME nature of Pb_2MnO_4, observed through magnetic and dielectric measurements under external pressures and magnetic and electric fields.

*Corresponding author: yang@mail.nsysu.edu.tw

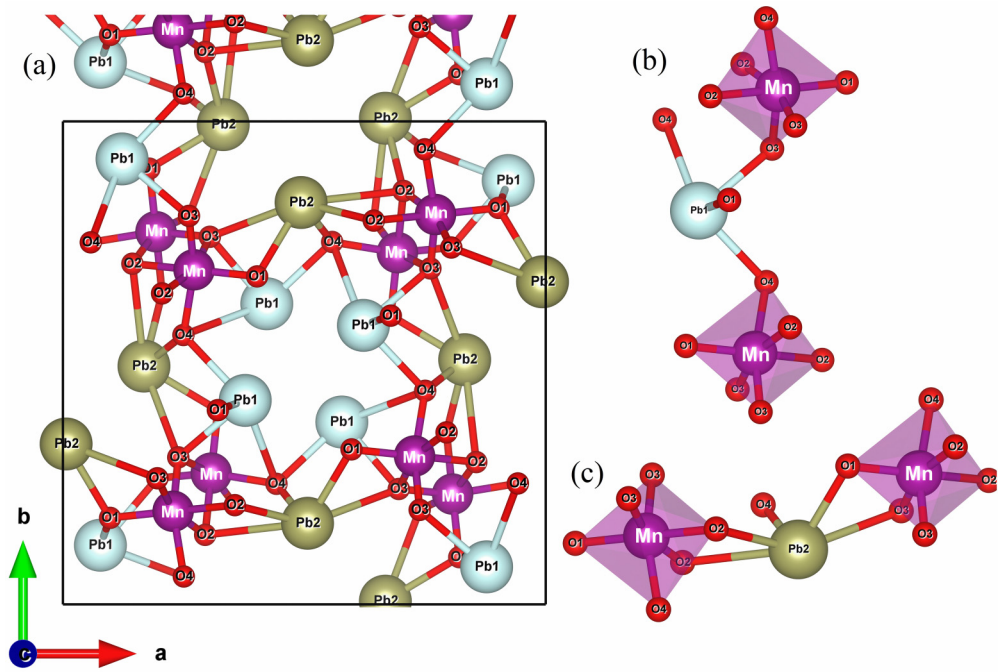

FIG. 1. (a) Schematic view of the crystal structure at room temperature in the *ab* plane. Bridging of Mn ions via (b) Pb(1) and (c) Pb(2) atoms, respectively. Crystal structure was drawn from the refinement .cif file using the VESTA software.

II. EXPERIMENTAL DETAILS

Polycrystalline Pb_2MnO_4 was prepared by the conventional solid-state reaction method [29]. Powder x-ray diffraction (XRD) measurements were done at room temperature using a Bruker D8 diffractometer equipped with the monochromator for Cu$-K_\alpha$ radiation. X-ray absorption spectroscopy (XAS) measurements were performed at the 20A beamline of National Synchrotron Radiation Research Center (NSRRC)-Taiwan. The dc and ac magnetic measurements utilized a commercially available Quantum Design MPMS-XL7 magnetometer, over the temperature (T) range of 2 to 300 K. High-pressure measurements were conducted in a piston-cylinder-type high-pressure apparatus designed for the MPMS-XL7 magnetometer with Daphne-7373 oil used as a pressure medium and a tin manometer. Specific-heat measurements were conducted on a physical property measurement system (PPMS, Quantum Design) and used the 2τ relaxation method. Both sides of the pellet were coated with conducting silver epoxy for transport measurements (pyro and dielectric). Complex dielectric permittivity was measured using an Agilent 4294A impedance analyzer with a home-made sample holder integrated to work with the PPMS. Dielectric measurements were conducted for the frequency window from 10 kHz to 1 MHz with the ac excitation voltage of 1 V. Isothermal ε' vs H was measured below and above T_N at 1 MHz. The polarization hysteresis (P-E) loops were obtained using the commercially available Radiant precision multiferroic II instrument. Field-dependent pyrocurrent measurements were acquired using the Keithley 6517B electrometer (shown in Supplemental Material, Fig. S4 [30]). A pulsed-field magnet was used for the high-field magnetization at the Megagauss Laboratory of the Institute for Solid State Physics of the University of Tokyo. Electric-field effects on the magnetization data were performed with a home-made sample holder integrated to work with the MPMS-XL7 magnetometer. Magnetization data were collected by simultaneously applying the electric field using the Keithley 6517B electrometer.

III. RESULTS AND ANALYSES

A. Structural analysis

Rietveld refinement of the room-temperature XRD data (shown in Supplemental Material, Fig. S1 [30]) confirms the tetragonal crystal structure with the $P\bar{4}2_1c$ space group and is consistent with previously published literature [29]. The room-temperature XAS spectrum reveals the Mn^{4+} oxidation state (shown in Supplemental Material, Fig. S2 [30]). The

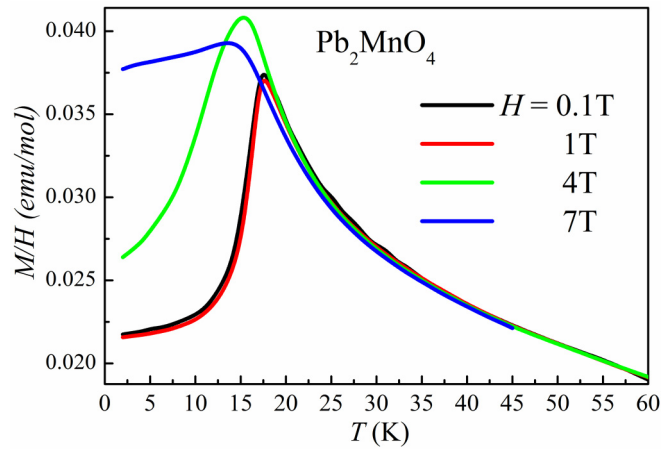

FIG. 2. M/H vs T curves for different applied fields for the temperature interval of 2 to 60 K.

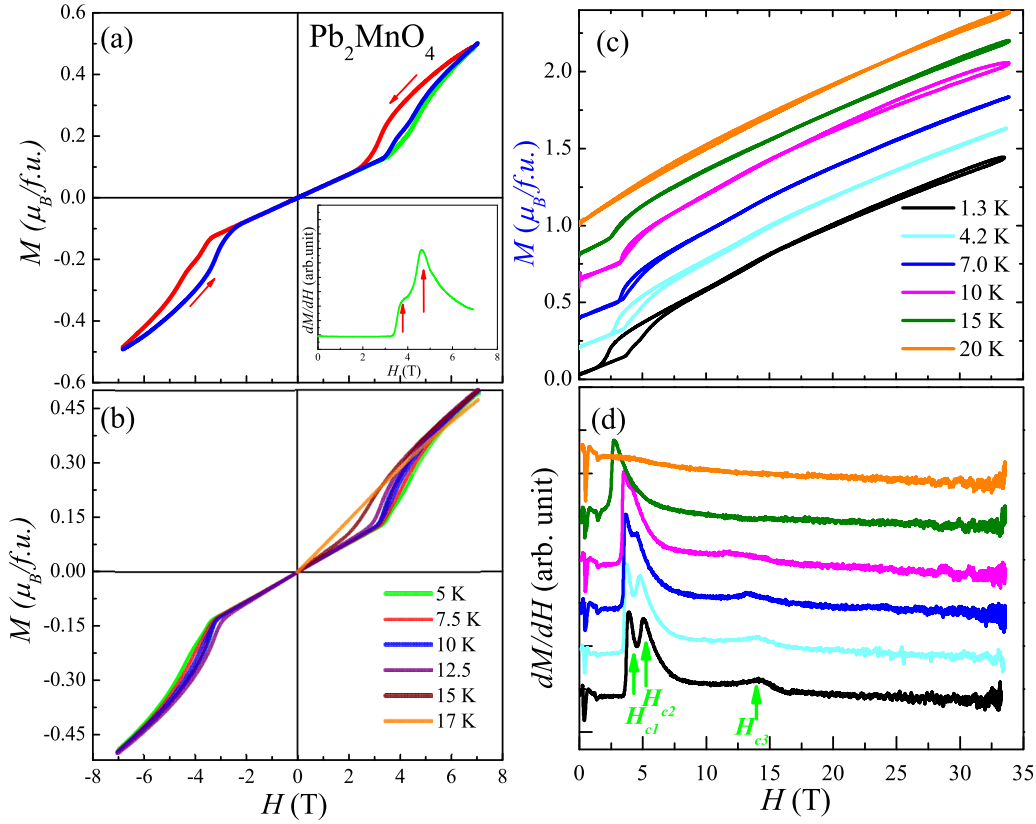

FIG. 3. (a) Isothermal *M*-*H* curve at 2 K; the inset shows the differential curves of virgin data. (b) Isothermal *M*-*H* curves at different temperatures and note that the hysteresis (denoted as a metamagnetic transition) only occurs at $T < T_N$ and $H > H_c$. (c) High field *M*-*H* curves at different temperatures up to 32 T; for clarity, data were stacked vertically with a shift of 0.2 μ_B/f.u. (d) *dM/dH* vs *H* curves derived from Fig. 3(c); peaks at H_{c1}, H_{c2}, and H_{c3} indicate the multiple metamagnetic transitions.

crystal structure was drawn from the Rietveld refinement pattern using VESTA software. The crystal structure [shown in Fig. 1(a)] consists of spin chains aligned along the *c* direction, formed by edge-sharing MnO_6 octahedra. Stereographically active lone pair Pb^{2+} ions have two crystallographic positions Pb(1) and Pb(2) in the lattice and contain two types of polyhedrons $Pb(1)O_5$ and $Pb(2)O_4$ with the tunnel structure along the *c* axis. Chemically inactive lone pair Pb^{2+} ions are projected in the tunnels, and Pb(2) is centered around (1/2, 0, *z*), forming the larger diameter of 4.3 Å, whereas Pb(1) tunnels center at (1/2,1/2, *z*) and form the smaller tunnel with a diameter of 3.7 Å. The Mn^{4+} (d^3; $S = 3/2$) ions are magnetically coupled via several intrachain and interchain magnetic interactions. The edge-shared Mn^{4+} ions in the intrachain have the shortest distance of 2.93 Å which favors the direct exchange interactions for Mn-Mn, whereas Mn^{4+} octahedral chains in the *ab* plane are isolated by the lone pair Pb^{2+} ions [as shown in Figs. 1(b) and 1(c)] with the Mn-Mn interchain distance ranging between 6.41 and 6.56 Å. Mn ions in the *ab* plane favor the super-superexchange interaction mediated via the Pb and oxygen ions.

B. Magnetic measurements

Dc magnetization measurements observed a sharp paramagnetic (PM) to AFM transition at $T_N = 17$ K and the obtained effective PM moment is consistent with published literature [29] (shown in Supplemental Material, Fig. S3 [30]). Figure 2 illustrates the temperature-dependent zero field-cooled (ZFC) magnetization for several different magnetic fields. Magnetization data under 1 T resemble those of 0.1 T magnetic data;

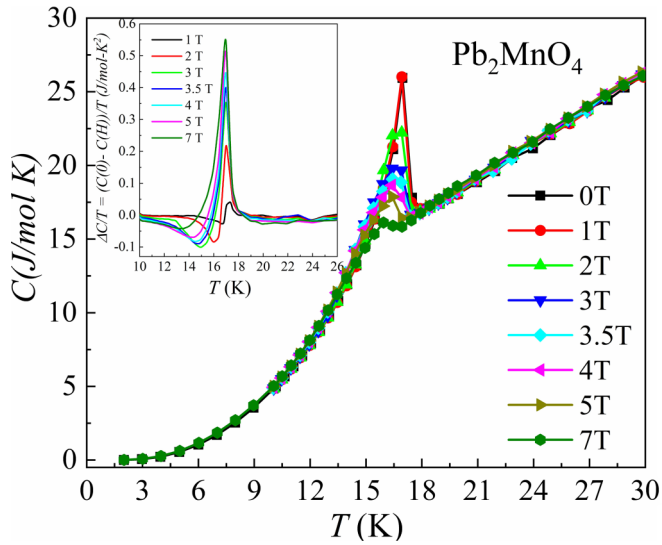

FIG. 4. *C* vs *T* curves with applied magnetic fields from 0 to 7 T; the inset shows the $\Delta C/T = [C(0) - C(H)]/T$ vs *T* curves for the applied fields from 0 to 7 T.

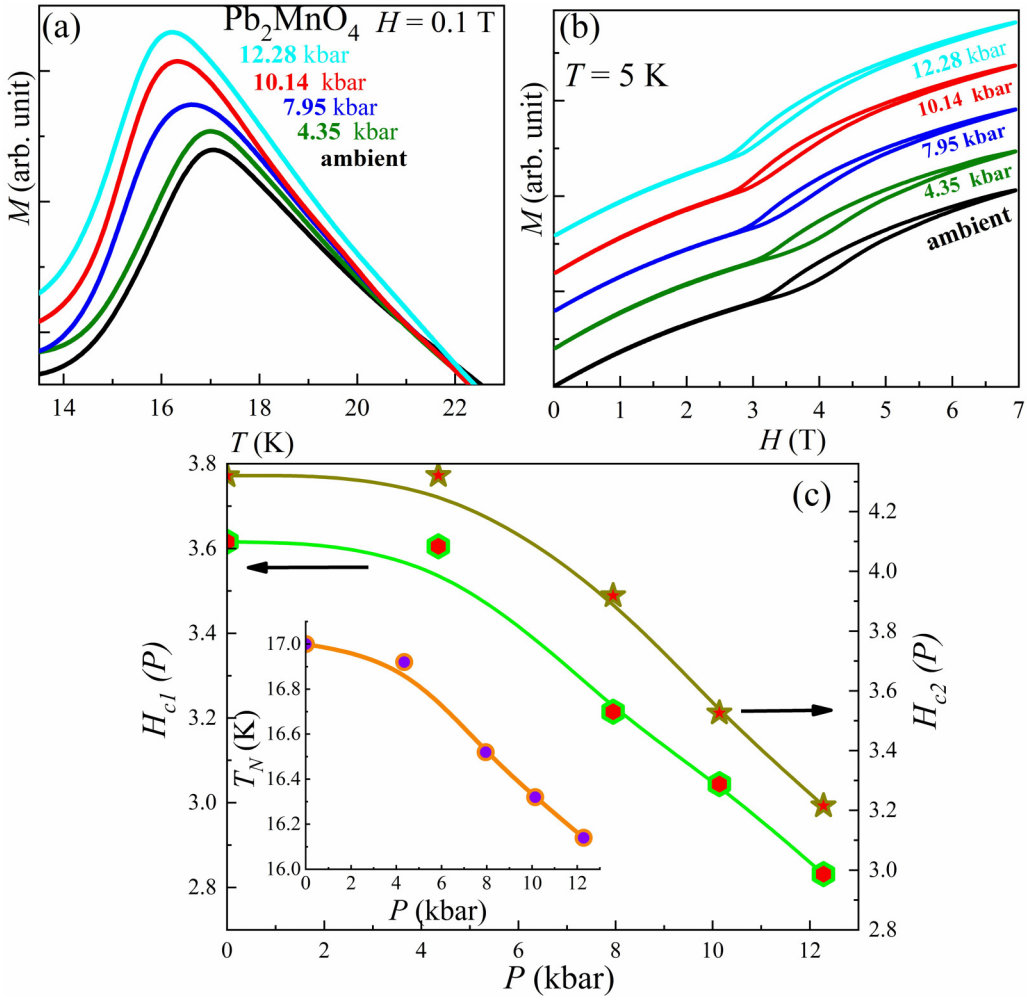

FIG. 5. (a) *M-T* curves measured at $H = 0.1$ T in ZFC protocol under different applied pressures up to 12.28 kbars. (b) Isothermal *M-H* curves at 5 K under different applied pressure up to 12.28 kbars; for clarity data are vertically shifted along the *y* axis. (c) Variation of H_{c1} and H_{c2} with respect to applied pressure; the inset shows the T_N vs *P* curve.

however, above 4 T there is an enhancement of susceptibility. With increasing field, the magnetization is trending to saturated, as seen for 7 T below T_N. All these features suggest the metamagnetic nature. Field-dependent magnetization (*M-H*) curves were performed at 2 K and are displayed in Fig. 3(a), to clarify the nature of the metamagnetic transition. Low-field *M-H* measurements observed a linear variation followed by a jump at a critical magnetic field for $H > 3.5$ T. In general, the jump in the isothermal magnetization indicates a metamagnetic transition. To gain further insight into the metamagnetic transitions, we also plotted the *dM*/*dH* vs *H* curves in the inset of Fig. 3(a). Two peaks are observed in the *dM*/*dH* vs *H* with one around 3.73 T and another at 4.65 T, which can be designed as H_{c1} and H_{c2}, respectively. The critical fields (H_{c1} and H_{c2}) decrease and eventually disappear as $T > T_N$. The AFM to metamagnetic transition has not been reported in literature until now. The polycrystalline sample orders as a 3D AFM, where the only magnetic ion responsible for the metamagnetic transition is the Mn^{4+}. To further understand the microscopic mechanism of the metamagnetic transition, a single crystal is required. Furthermore, the *M-H* curves show a pronounced double hysteresis and the width of the hysteresis decreases with increasing temperature [as seen in Fig. 3(b)], and this might be attributed to the domain-wall effect.

The highest achieved magnetization value at 2 K is 0.44 μ_B/f.u. within our available experimental fields of 7 T; this is only ∼16% of the total magnetization value of the Mn^{4+} ion. The magnetization might continue to grow monotonically with increasing magnetic field, or it might show additional metamagnetic transitions at higher fields. To further clarify this possibility, high-field magnetic measurements were conducted, as shown in Fig. 3(c). The characteristic feature at low fields is consistent with that of the low-field superconducting quantum interference device measurements. It is noted that the *dM*/*dH* vs *H* curve in Fig. 3(d) reveals a weak and broad transition at 13.5 T indicated as H_{c3}, which disappears with increasing temperatures. Further studies are required to understand these complex metamagnetic transitions.

C. Magnetic-field-dependent specific-heat measurements

Specific-heat measurements between 2 and 30 K at zero field and in applied fields are shown in Fig. 4. A prominent

λ-shaped anomaly was observed at zero field at T_N in the C vs T plot. This peak in $C(T)$ gives clear evidence of long-range order. Furthermore, the peak at zero field is sharp, indicating a high quality of the sample. With the increasing dc magnetic field, the peak in the C vs T is gradually suppressed and shifts toward lower temperatures, which is a generic feature for AFM materials. At temperatures below 12 K (also see the inset of Fig. 4), the $C(T)$ data of 0 and 7 T are nearly identical, which indicates that there is no excess entropy under the application of magnetic field up to $H = 7$ T. The $\Delta C/T$ vs T curves for various applied fields shown in the inset of Fig. 4 exhibit a dip anomaly for $T \leqslant T_N$. The dip feature below T_N shows a rapid shift towards lower temperatures with increasing H, while it increases in temperature as $H > H_c$. With a further increase in H, this dip feature begins to diminish. This nonmonotonic change matches the existence of metamagnetic transitions as shown in Fig. 3.

D. Effects of external pressure on magnetic properties

As mentioned, Pb_2MnO_4 belongs to the multipiezo family with piezoelectric ($P\bar{4}2_1c$) and piezomagnetic ($P\bar{4}2_1c'$) space groups [29], which makes Pb_2MnO_4 an excellent candidate to investigate the influence of external perturbations on the magnetic and magnetoelectric phenomena. The effects of external pressure on the T_N and the metamagnetic transitions have been illustrated in Figs. 5(a) and 5(b). The T_N [∼4.8%; see inset of Fig. 5(c)] is decreased with increasing pressure. The critical fields H_{c1} and H_{c2} to induce metamagnetic transitions are decreased by ∼21.6 and 25.5% with pressure up to 12.2 kbars. Unfortunately, the detailed directional dependent piezomagnetic response cannot be specified by these polycrystalline measurements.

E. Magnetic-field-dependent dielectric properties

The ε' vs T curves for the different frequencies (10 kHz to 1 MHz) are illustrated in Fig. 6(a) for the temperature ranges of 7–300 K. As shown in Fig. 6(a), a frequency dispersion is observed for ε' near room temperature. With decreasing temperature, ε' decreases drastically till a steplike drop occurs followed by a plateau; however, with increasing frequency, there is an observed softening of the steplike transition. The observed ε' (∼18) and tanδ (∼10^{-1}, not shown here) values are low, which excludes the extrinsic parasitic contribution to the observed dielectric variations. An interesting phenomenon was observed in Fig. 6(b) at low temperature, where a clear ε' anomaly is observed at $T_E = 17$ K. This anomaly occurs at the onset of AFM transition and suggests that the magnetic interactions might be responsible for the dielectric response. The frequency independent dielectric anomaly further indicates the intrinsic nature of the dielectric ordering. It is also interesting to mention that temperature-dependent neutron-diffraction measurements down to 1.5 K did not observe any crystal-structural transitions; this then rules out the possibility of a structure-induced dielectric anomaly at T_E [29]. The nature of the dielectric anomaly at T_E can be described by an Einstein-type lattice dielectric polarizability distribution

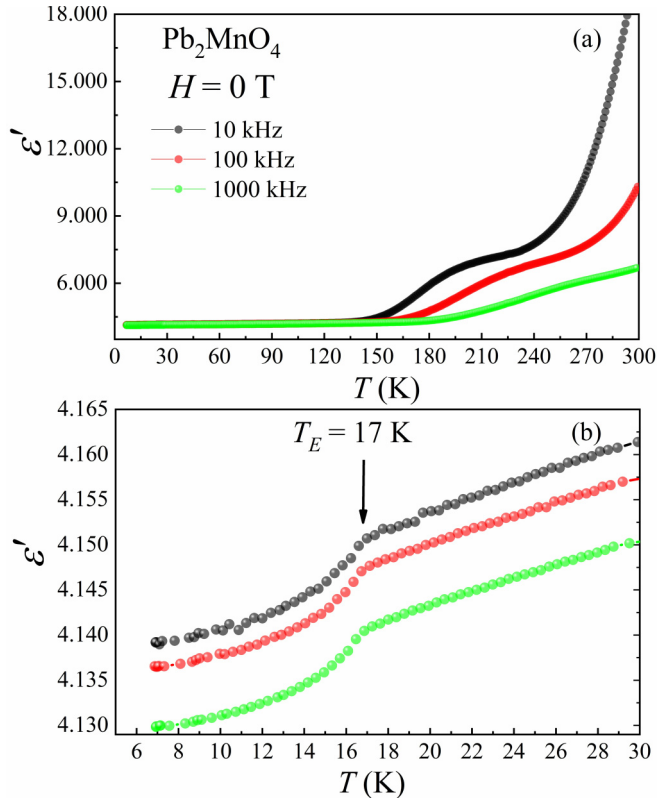

FIG. 6. (a) ε' vs T with different frequencies and (b) in the low-temperature (7–30-K) region.

function and is given by Refs. [20,21,26,31,32]:

$$(T) = (0) + \frac{A}{[\exp(T^*/T) - 1]}$$

where A is a constant and $T* = h\upsilon_T/k_B$ represents the characteristic temperature associated with transverse phonon mode frequency (υ_T). The above equation has a limitation: it considers only a single transverse optical phonon, and it is valid for the specific crystallographic axis that depends on the symmetry of that particular crystal lattice. Despite this limitation, the equation was fitted to several polycrystalline samples [24,33]. In that case, the obtained υ_T represents the average phonon frequency weighted over all the possible phonons. A satisfactory fit of the equation to the experimental data above T_E can be seen in Fig. 7(a) and the observed lattice dielectric constant deviates near T_N. The obtained fitting parameters lead to the υ_T of 26.5 cm^{-1}, and this value is one order of magnitude smaller than the well-known AFM MnO and MnF_2 piezomagnetic systems [20] and can be attributed to the polycrystalline nature of the sample. A similar dielectric anomaly is observed in many ME materials, e.g., $RMnO_3$, $Y_2Cu_2O_5$, $BiMnO_3$, MnO, MnF_2, $BaMnF_4$, $GeCo_2O_4$, $TbFe_3(BO_3)_4$, binary $\alpha - Mn_2O_3$, and hybrid Cr(II) phosphonate [12–14,18,21,23,24,27,31,32,34], where the magnetoelastic coupling between the spin and lattice results in higher-order ME coupling. The effects of the magnetic field on the T_E ε' vs T curves under different magnetic fields (0–9 T) are plotted in Fig. 7(b). There is no change of ε' vs T data up to 2 T; however, there is a

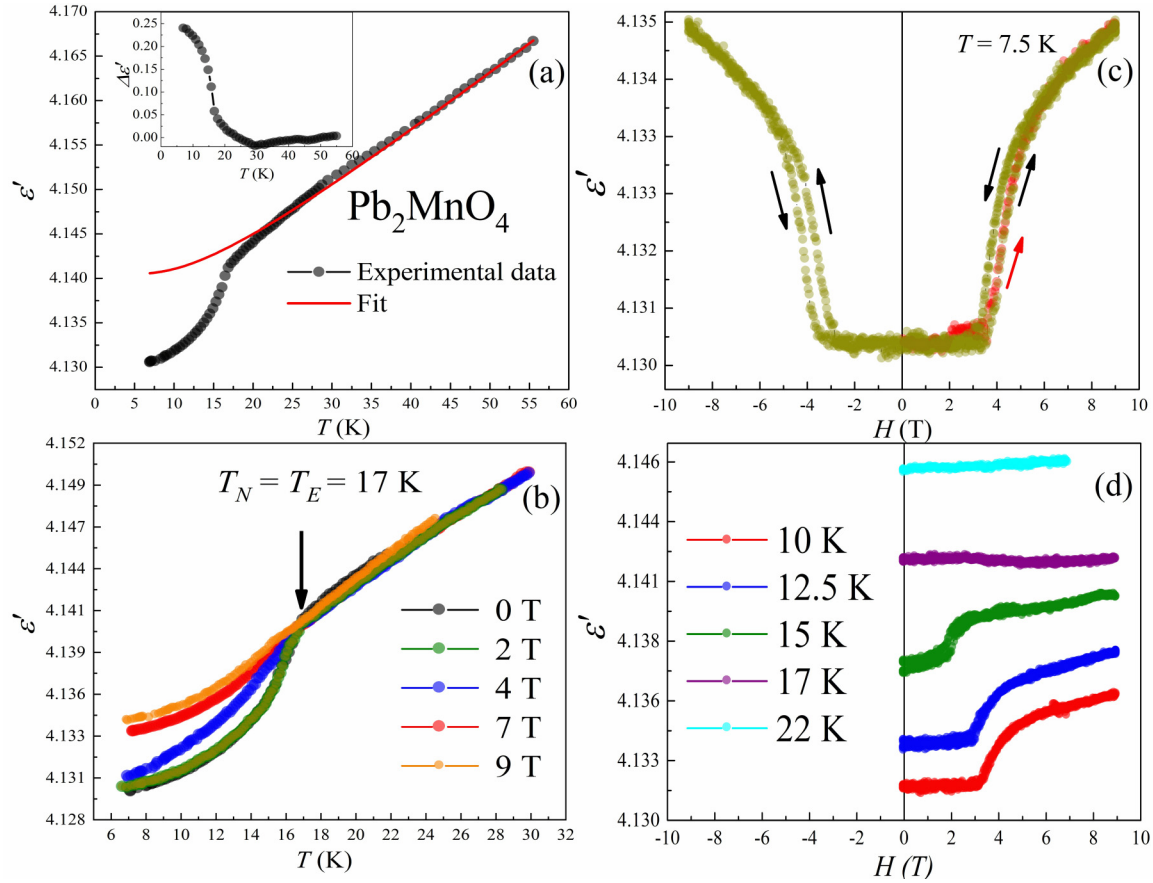

FIG. 7. (a) ε' vs T data for 1-MHz data; the solid line indicates the fit to the Einstein-type distribution; the inset shows the $\Delta\varepsilon'$ vs T data. (b) ε' vs T curves for different applied magnetic fields under the frequency of 1 MHz. (c) Isothermal ε' vs H curve for $T = 7.5$ K. (d) Isothermal ε' vs H curves at different temperatures.

noticeable change at 4 T as seen in ε' vs T curves, and the droplike feature of ε' near T_N appears to be moving towards lower temperatures as the applied field increases. For the 9-T data, it has almost disappeared and a linear decrease of ε' was observed down to the lowest measured temperature. The features of ε' vs T curves resemble those of the magnetization data. To further address this behavior, isothermal MD data were measured at different temperatures [Figs. 7(c) and 7(d)]. The ε' is unresponsive for fields up to 4.3 T, but with the increasing field a rapid upturn denoted as ε'_c is noticed coupled with finite hysteresis with respect to the field sweeping directions. Moreover, the ε'_c transition temperature shifts to lower fields with increasing temperature and eventually vanishes near T_N. It is interesting that the field at which the dielectric anomaly occurred matches with the onset of the metamagnetic transitions, which signifies the existence of a coupling between the magnetic and dielectric response via a magnetoelastic coupling.

F. Effects of electric field on magnetoelectric properties

The measurements from Fig. 7 indirectly establish the existence of the MD effect that was mediated by the magnetoelastic coupling. However, direct coupling between the magnetic and electric entities was investigated by studying the electric-field influence on the metamagnetic transition and has been illustrated in Fig. 8(a). At first glance, no influence of the external electric field on the metamagnetic transition can be observed. However, by plotting $\Delta M\% = [(M_E - M_0)/M_0] \times 100$ as seen in the inset of Fig. 8(a) a clear drop at the critical field denoted as ΔM_c can be seen and is enhanced by increasing the external poling field. This result indicates that the electric field can undoubtedly influence the metamagnetic transition in Pb_2MnO_4. However, no induced ferroelectricity was observed when an external magnetic field was applied as shown as P-E loops in Fig. 8(b). Usually, for piezo systems, external perturbations result in noticeable effects of the sample's properties. The deviation between theoretical predictions and the experimental data might be accounted for by the powder nature of the samples, as the directional piezo properties might be averaged out over the randomness.

IV. DISCUSSIONS

The ME phenomenon of the Pb_2MnO_4 sample is summarized in Fig. 9(a), where the H_{c1}, H_{c2}, H_{c3}, ε'_c, and ΔM_c data points have been selected from Figs. 3, 7, and 8, respectively. As demonstrated by the ME phase diagram, the dielectric response appears below T_N and is nicely coupled with the metamagnetic transitions. The simultaneous appearance of the dielectric transition, as well as the magnetic ordering, reflects

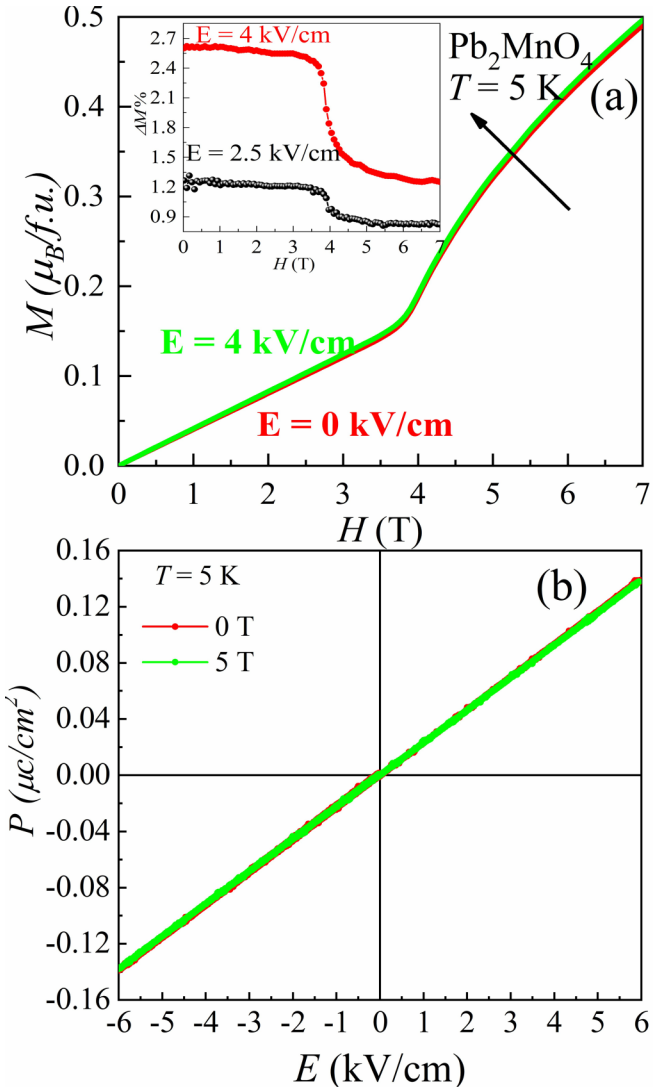

FIG. 8. (a) M-H curves at 5 K under the electric fields for 0 and 4 kV/cm, respectively; the inset shows the $\Delta M\% = [M(E)-M(0)]/M(0) \times 100$ vs H curves for 2.5 and 4 kV/cm, respectively. (b) P vs H curves for the applied magnetic field of 0 and 5 T, respectively; the inset shows the M/H vs T curves for different electric fields.

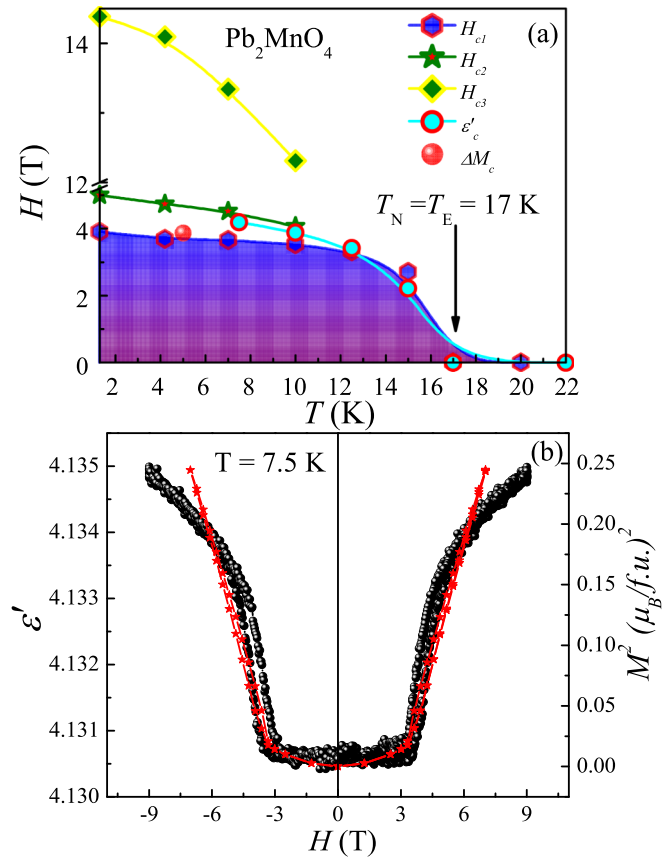

FIG. 9. (a) Magnetoelectric phase diagram of Pb_2MnO_4 determined by M vs H, ε' vs T, and $\Delta M\%$ vs H, respectively; the arrow at 17 K indicates the magnetic (T_N) and dielectric ordering (T_E) temperature. (b) ε' (in black) and M^2 (in red) vs H curve measured at 7.5 K; the scaling between ε' with M^2 signifies the spin-lattice coupling.

the coupling between the crystal lattice and magnetism in this system. From a structural point of view, the asymmetric coordination of oxygen ions at the Pb(1) and Pb(2) sites due to stereographically project lone pair electrons creates the electric dipoles. Kimber and Attfield suggested that the electrical dipoles lie parallel to the *ab* plane [29]. Within the *ab* plane, the antiparallel orientations of the electrical dipoles cancel each other and result in a net zero electrical dipole moment. On the other hand, the magnetic structure from temperature-dependent neutron refinements suggests that the Mn magnetic moments orient in the *ab* plane with AFM interactions along the *c* direction. The dominant magnetic interactions happen between the Mn ions within the Mn spin chain. However, in the *ab* plane, the magnetic dipoles at Mn sites are bridged by the super-superexchange interaction mediated via lone pair Pb^{2+} ions, which are the source for the electric dipole moments. The intimate link between the magnetic and electrical dipoles in the *ab* plane via magnetoelastic coupling might trigger a weak higher-order ME coupling in this material. Recently published neutron-diffraction data support the existence of the magnetoelastic coupling, where the magnetic exchange interactions below T_N are enhanced with a decrease of the bond length and the bond angle between the magnetic Mn ions [35]. A similar ME response has also been observed in the hexagonal $RMnO_3$ systems, where the AFM interaction in the hexagonal basal planes invokes the spin-lattice coupling that is reflected in the ME measurements [18]. Terahertz and infrared spectroscopic studies have further confirmed the significant coupling of the phonon and magnon branches that are responsible for the higher-order ME coupling observed in the piezomagnetic $YMnO_3$ system [36].

Although the nonpolar symmetry restricts the multiferroic mechanism in Pb_2MnO_4, an occurrence of weak higher-order ME coupling has been predicted in the multipiezo systems. From the mean-field approximation, the magnetic exchange striction in such a system is invoked to yield the $\varepsilon^m \propto$ spin pair-correlation function, where ε^m is the magnetic contribution of dielectric response. Several polar and nonpolar magnetoelectric systems have already been found to exhibit this higher-order ME coupling. The magnetoelastic couplings

in piezomagnetic MF_2 (M = Mn, Fe, and Ni) and MnO systems show the phonon spectrum renormalization near T_N induced by AFM ordering [37]. Further neutron-diffraction studies reveal the coupling of lattice strains with the square of the order parameter of the AFM phase transition [22]. The evidence of higher-order ME effect ($\Delta\varepsilon \propto M^2$) in the present system shown in Fig. 9(b) implies that the exchange striction might be the responsible mechanism for the ME properties. Exchange striction stretches or elongates the bond between the Mn-O-Pb-O-Mn in the *ab* plane during the AFM ordering, which results in a shifting of the phonon frequency and a change in the dielectric constant near T_N. Additional enhancement at metamagnetic transitions is also observed for this ME coupling, where the external field forces the metamagnetic transition, which then alters the lattice polarizability of the Pb_2MnO_4. Although external pressures and electric fields both exhibited a noticeable response near the metamagnetic transition, a clear picture of stress-mediated coupling between the piezo coefficients deserves further study. Either single-crystal or thin-film samples are necessary to quantify the directional dependent multipiezo response.

V. SUMMARY

The critical findings on Pb_2MnO_4 in this paper are summarized as follows:

(1) The 3D antiferromagnetic ordering transition occurs at $T_N \sim 17$ K, and below T_N the magnetic-field-induced multiple metamagnetic transitions appear for $H > 3.5$ T.

(2) T_N decreases with the application of external pressure, whereas much stronger pressure influence is noticed at both H_{c1} and H_{c2}.

(3) A dielectric anomaly is observed near T_N under $H = 0$ and is clearly affected by applying magnetic field as $H > 3.5$ T, indicating the coupling between magnetic-field-induced metamagnetic transition and MD effect.

(4) The electric field shows a noticeable effect on the metamagnetic transition.

(5) The scaling of $\Delta\varepsilon \propto M^2$ supports the evidence of weak higher-order ME coupling in the acentric and nonpolar Pb_2MnO_4.

ACKNOWLEDGMENTS

This work was supported by the Ministry of Science and Technology, Taiwan under Grants No. 106-2112-M-110-013-MY3 and No. 106-2112-M-009-002. The authors thank C. Y. Wu for help with specific-heat measurements and NSRRC for XAS measurements.

[1] W. Eerenstein, N. D. Mathur, and J. F. Scott, Nature (London) **442**, 759 (2006).
[2] F. Manfred, J. Phys. D **38**, R123 (2005).
[3] T. Lottermoser, T. Lonkai, U. Amann, D. Hohlwein, J. Ihringer, and M. Fiebig, Nature (London) **430**, 541 (2004).
[4] P. Ghosez and J.-M. Triscone, Nat. Mater. **10**, 269 (2011).
[5] H. J. Xiang, E. J. Kan, Y. Zhang, M. H. Whangbo, and X. G. Gong, Phys. Rev. Lett. **107**, 157202 (2011).
[6] P. Barone, K. Yamauchi, and S. Picozzi, Phys. Rev. B **92**, 014116 (2015).
[7] K. F. Wang, J. M. Liu, and Z. F. Ren, Adv. Phys. **58**, 321 (2009).
[8] H. Katsura, N. Nagaosa, and A. V. Balatsky, Phys. Rev. Lett. **95**, 057205 (2005).
[9] C.-H. Lee, C.-W. Wang, Y. Zhao, W.-H. Li, J. W. Lynn, A. B. Harris, K. Rule, H.-D. Yang, and H. Berger, Sci. Rep. **7**, 6437 (2017).
[10] K. D. Chandrasekhar, J. K. Murthy, J. Y. Lin, H. C. Wu, W. J. Tseng, A. Venimadhav, and H. D. Yang, Phys. Rev. B **94**, 205143 (2016).
[11] X. Z. Lu, M. H. Whangbo, S. Dong, X. G. Gong, and H. J. Xiang, Phys. Rev. Lett. **108**, 187204 (2012).
[12] M. S. Seehra and R. E. Helmick, Phys. Rev. B **24**, 5098 (1981).
[13] G. Nénert, U. Adem, E. M. Bauer, C. Bellitto, G. Righini, and T. T. M. Palstra, Phys. Rev. B **78**, 054443 (2008).
[14] M. Chandra, S. Yadav, R. J. Choudhary, R. Rawat, A. K. Sinha, M.-B. Lepetit, and K. Singh, Phys. Rev. B **98**, 104427 (2018).
[15] S. Seki, X. Z. Yu, S. Ishiwata, and Y. Tokura, Science **336**, 198 (2012).
[16] J. Cong, K. Zhai, Y. Chai, D. Shang, D. D. Khalyavin, R. D. Johnson, D. P. Kozlenko, S. E. Kichanov, A. M. Abakumov, A. A. Tsirlin, L. Dubrovinsky, X. Xu, Z. Sheng, S. V. Ovsyannikov, and Y. Sun, Nat. Commun. **9**, 2996 (2018).
[17] H. C. Wu, K. D. Chandrasekhar, J. K. Yuan, J. R. Huang, J. Y. Lin, H. Berger, and H. D. Yang, Phys. Rev. B **95**, 125121 (2017).
[18] T. Katsufuji, S. Mori, M. Masaki, Y. Moritomo, N. Yamamoto, and H. Takagi, Phys. Rev. B **64**, 104419 (2001).
[19] Y. Aikawa, T. Katsufuji, T. Arima, and K. Kato, Phys. Rev. B **71**, 184418 (2005).
[20] M. S. Seehra, R. E. Helmick, and G. Srinivasan, J. Phys. C **19**, 1627 (1986).
[21] U. Adem, G. Nenert, Arramel, N. Mufti, G. R. Blake, and T. T. M. Palstra, Eur. Phys. J. B **71**, 393 (2009).
[22] C. Tapan, N. I. Gail, O. Bachir, and C. H. Thomas, J. Phys.: Condens. Matter **22**, 316001 (2010).
[23] N. Mufti, G. R. Blake, M. Mostovoy, S. Riyadi, A. A. Nugroho, and T. T. M. Palstra, Phys. Rev. B **83**, 104416 (2011).
[24] P. T. Barton, M. C. Kemei, M. W. Gaultois, S. L. Moffitt, L. E. Darago, R. Seshadri, M. R. Suchomel, and B. C. Melot, Phys. Rev. B **90**, 064105 (2014).
[25] G. Lawes, A. P. Ramirez, C. M. Varma, and M. A. Subramanian, Phys. Rev. Lett. **91**, 257208 (2003).
[26] D. L. Fox, D. R. Tilley, J. F. Scott, and H. J. Guggenheim, Phys. Rev. B **21**, 2926 (1980).
[27] M. S. Seehra and R. E. Helmick, J. Appl. Phys. **55**, 2330 (1984).
[28] S. A. Ivanov, A. A. Bush, M. Hudl, A. I. Stash, G. André, R. Tellgren, V. M. Cherepanov, A. V. Stepanov, K. E. Kamentsev, Y. Tokunaga, Y. Taguchi, Y. Tokura, P. Nordblad, and R. Mathieu, J. Mater. Sci. Mater. Electron. **27**, 12562 (2016).
[29] S. A. J. Kimber and J. P. Attfield, J. Mater. Chem. **17**, 4885 (2007).

[30] See Supplemental Material at http://link.aps.org/supplemental/10.1103/PhysRevB.99.195129 for XRD, dc, and ac magnetization and pyroelectric measurements.
[31] J. F. Scott, Phys. Rev. B **16**, 2329 (1977).
[32] U. Adem, L. Wang, D. Fausti, W. Schottenhamel, P. H. M. van Loosdrecht, A. Vasiliev, L. N. Bezmaternykh, B. Büchner, C. Hess, and R. Klingeler, Phys. Rev. B **82**, 064406 (2010).
[33] J. K. Harada, L. Balhorn, J. Hazi, M. C. Kemei, and R. Seshadri, Phys. Rev. B **93**, 104404 (2016).
[34] Jan-Willem G. Bos, C. V. Colin, and T. T. M. Palstra, Phys. Rev. B **78**, 094416 (2008).
[35] C. Yin, E. Solana-Madruga, H. Chen, and J. P. Attfield, J. Solid State Chem. **269**, 336 (2019).
[36] C. Kadlec, V. Goian, K. Z. Rushchanskii, P. Kužel, M. Ležaić, K. Kohn, R. V. Pisarev, and S. Kamba, Phys. Rev. B **84**, 174120 (2011).
[37] R. Schleck, Y. Nahas, R. P. S. M. Lobo, J. Varignon, M. B. Lepetit, C. S. Nelson, and R. L. Moreira, Phys. Rev. B **82**, 054412 (2010).